RESEARCH ARTICLE

In Vivo E2F Reporting Reveals Efficacious Schedules of MEK1/2–CDK4/6 Targeting and mTOR–S6 Resistance Mechanisms

Jessica L.F. Teh[1], Phil F. Cheng[2], Timothy J. Purwin[1], Neda Nikbakht[3], Prem Patel[1], Inna Chervoneva[4,5], Adam Ertel[1], Paolo M. Fortina[1], Ines Kleiber[2], Kim HooKim[6], Michael A. Davies[7], Lawrence N. Kwong[8], Mitch P. Levesque[2], Reinhard Dummer[2], and Andrew E. Aplin[1,3,5]

ABSTRACT   Targeting cyclin-dependent kinases 4/6 (CDK4/6) represents a therapeutic option in combination with BRAF inhibitor and/or MEK inhibitor (MEKi) in melanoma; however, continuous dosing elicits toxicities in patients. Using quantitative and temporal *in vivo* reporting, we show that continuous MEKi with intermittent CDK4/6 inhibitor (CDK4/6i) led to more complete tumor responses versus other combination schedules. Nevertheless, some tumors acquired resistance that was associated with enhanced phosphorylation of ribosomal S6 protein. These data were supported by phospho-S6 staining of melanoma biopsies from patients treated with CDK4/6i plus targeted inhibitors. Enhanced phospho-S6 in resistant tumors provided a therapeutic window for the mTORC1/2 inhibitor AZD2014. Mechanistically, upregulation or mutation of *NRAS* was associated with resistance in *in vivo* models and patient samples, respectively, and mutant NRAS was sufficient to enhance resistance. This study utilizes an *in vivo* reporter model to optimize schedules and supports targeting mTORC1/2 to overcome MEKi plus CDK4/6i resistance.

SIGNIFICANCE: Mutant BRAF and NRAS melanomas acquire resistance to combined MEK and CDK4/6 inhibition via upregulation of mTOR pathway signaling. This resistance mechanism provides the preclinical basis to utilize mTORC1/2 inhibitors to improve MEKi plus CDK4/6i drug regimens. *Cancer Discov; 8(5); 1–14. ©2018 AACR.*

See related commentary by Sullivan, p. 532.

See related article by Romano et al., p. 556.

[1]Department of Cancer Biology, Thomas Jefferson University, Philadelphia, Pennsylvania. [2]Department of Dermatology, University of Zurich Hospital, Zurich, Switzerland. [3]Department of Cutaneous Biology and Dermatology, Thomas Jefferson University, Philadelphia, Pennsylvania. [4]Division of Biostatistics, Department of Pharmacology and Experimental Therapeutics, Thomas Jefferson University, Philadelphia, Pennsylvania. [5]Sidney Kimmel Cancer Center, Thomas Jefferson University, Philadelphia, Pennsylvania. [6]Department of Pathology, Anatomy and Cell Biology, Thomas Jefferson University, Philadelphia, Pennsylvania. [7]Department of Melanoma Medical Oncology, Division of Cancer Medicine, The University of Texas MD Anderson Cancer Center, Houston, Texas. [8]Department of Translational Molecular Pathology, The University of Texas MD Anderson Cancer Center, Houston, Texas.

INTRODUCTION

Cyclin-dependent kinase 4/6 inhibitors (CDK4/6i) such as palbociclib (PD0332991), ribociclib (LEE011), and abemaciclib (LY2835219) are highly selective and have gained FDA approval/breakthrough therapy designation in estrogen receptor (ER)–positive/HER2-negative breast cancer in combination with aromatase inhibitors or the selective estrogen receptor degrader fulvestrant (1). Although immunotherapies and BRAF/MEK–targeted inhibitors have been FDA approved for the treatment of advanced-stage cutaneous melanoma, these therapies have limitations, and more effective treatment options are still required.

Aberrant cell-cycle progression is a hallmark of cancer and in melanoma is driven by mutant BRAF/NRAS–mediated upregulation of cyclin D1, amplification of cyclin D1, and loss of expression of the cyclin-dependent kinase inhibitor p16INK4A (2). These mechanisms lead to enhanced activity of CDK4/6 in the early-G_1 stage of the cell cycle. CDK4/6i treatment alone produces cytostatic effects in tumors and needs to be combined with other agents such as BRAF inhibitors (BRAFi) and MEK1/2 inhibitors (MEKi). Trials utilizing CDK4/6i alone or in combination are under way in melanoma (3–5), but their use needs to be optimized, and mechanisms

of acquired resistance are not known. In addition, continuous dosing of patients with CDK4/6i results in dose-limiting toxicities including neutropenia (6), and combinatorial inhibitor approaches can yield unique sets of toxicities. A key current question is how to maximize effects of CDK4/6i-based combinations while minimizing toxicities (3).

In vivo reporter models have been established to quantitatively analyze the response and resistance to targeted therapies selectively in the tumor and in a temporal manner (7, 8). In this study, we evaluated combination schedules with intermittent dosing of MEKi and/or CDK4/6i *in vivo* in melanoma models. We assessed combination schedules for their effects on tumor growth and E2F pathway inhibition. In addition, we characterized mechanisms of acquired resistance that arise from each schedule. Our studies identify resistance to MEK1/2–CDK4/6 targeting associated with molecular alterations in *NRAS* and upregulation of ribosomal S6 protein (RPS6). These findings were supported by analysis of clinical trial samples. Targeting the resistance-associated pathway using mTORC1/2 inhibitors led to enhanced apoptosis in MEKi–CDK4/6i-resistant cells and reduced tumor growth *in vivo*. Our findings provide new insight to scheduling and resistance to MEK1/2–CDK4/6 targeting and provide second-line treatment strategies for MEKi–CDK4/6i-resistant melanoma.

RESULTS

Continuous MEKi Treatment and Intermittent CDK4/6i Treatment Leads to Complete Responses *In Vivo*

To test optimal scheduling of MEKi plus CDK4/6i, we utilized a mutant BRAF 1205Lu model expressing an E2F-driven luciferase reporter and constitutive tdTomato fluorescent protein. Although continuous dosing of both drugs is effective in preclinical models (9), this regimen is not well tolerated in patients (4, 5, 10). On the basis of the intermittent dosing of CDK4/6i in breast cancer trials (10), we designed three scheduling arms: (i) continuous MEKi with intermittent CDK4/6i (3 weeks on/1 week off); (ii) continuous CDK4/6i with intermittent MEKi (3 weeks on/1 week off); and (iii) intermittent scheduling of both therapies (3 weeks on/1 week off; Fig. 1A). Our previous studies with this model showed that vehicle-treated tumors reach 800 mm^3 within 25 days (9). Of the three arms, the intermittent schedule of both therapies was the least effective with tumor regrowth during drug treatment and partial response to

retreatment following drug holidays. By the third cycle of treatment (days 56–77), the majority of tumors no longer responded to the combination therapy, suggesting a drug-tolerant state. More-effective tumor growth inhibition was observed with continuous dosing of either CDK4/6i or MEKi with intermittent dosing of the other drug. Of these two arms, continuous MEKi with intermittent CDK4/6i achieved statistical significance when compared with the intermittent schedule arm by both tumor volume measurement and tdTomato detection (Fig. 1B; Supplementary Fig. S1) and gave more complete responses as observed by nonpalpable tumors (Fig. 1A). Furthermore, residual tumors showed low levels of proliferation markers and a high number of apoptotic cells in the continuous MEKi intermittent CDK4/6i arm (Fig. 1C and D), but only a few tumors acquired resistance in this arm and statistical significance was not reached. Mouse weights were comparable across the three arms with modest decreases in the continuous CDK4/6i arm that reached statistical significance at day 66 (Fig. 1E), consistent with toxicities seen in preclinical and clinical studies (10). No significant toxicities in the various scheduling arms were observed with
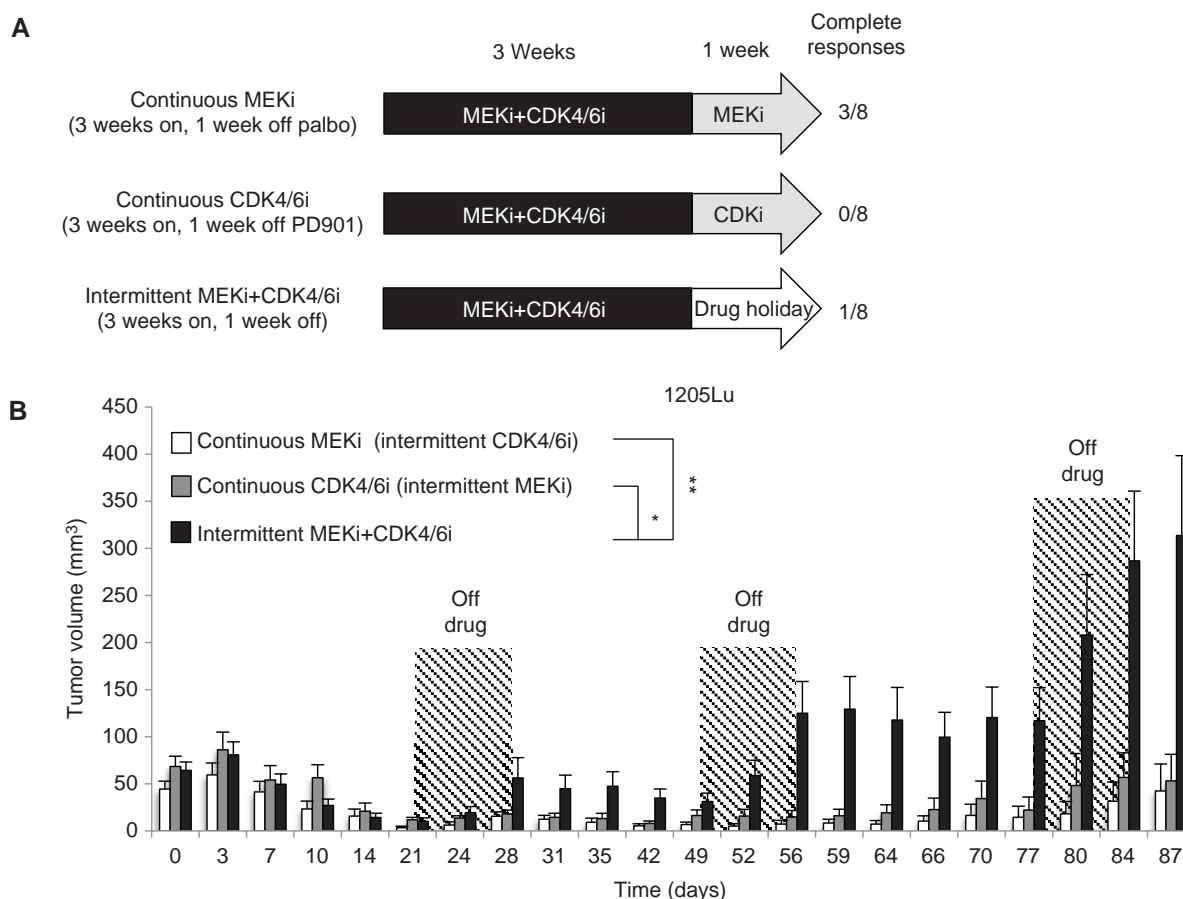
Figure 1. Comparison of continuous single-agent and intermittent dosing schedules in 1205Lu reporter xenografts. **A,** Mice bearing 1205Lu reporter xenografts were dosed with continuous MEKi + intermittent (3 weeks on/1 week off) palbociclib, continuous palbociclib + intermittent (3 weeks on/1 week off) PD0325901, and both drugs intermittently (3 weeks on/1 week off). Number of complete responses in each individual schedule is indicated. **B,** Average tumor volume in three scheduling arms measured by digital caliper (error bars = SEM, $n = 8$; **, $P < 0.001$; *, $P < 0.027$). Shaded area represents a 1-week drug holiday (single agent or combination). (*continued on following page*)

regards to anemia and neutropenia (Supplementary Fig. S2). Overall, the continuous MEKi with intermittent CDK4/6i treatment arm was the most effective schedule with regard to delaying melanoma tumor growth.

E2F Reactivation Associates with Resistance

Concurrent with tumor growth analysis, we also measured E2F luciferase to temporally quantitate pathway activation status. During the 3-week MEKi plus CDK4/6i lead-in consistent across all three arms, E2F activity normalized to tumor size was suppressed (Fig. 2A–C). The continuous MEKi-intermittent CDK4/6i schedule gave lowest overall tumor growth, but two resistant tumors emerged (Fig. 2A). Tumor #2 showed reactivation of luciferase reporter activity during the first two rounds of CDK4/6i release and was dramatically activated during the third round of treatment associating E2F-regulated activity with tumor progression. Continuous CDK4/6i with intermittent MEKi maintained E2F activity at low levels; however, rapid regrowth of tumors was associated with E2F reactivation (Fig. 2B). In the intermittent MEKi plus CDK4/6i schedule, we observed rapid reactivation of the E2F

pathway within the first drug holiday in multiple tumors (#1, #2, #3, and #7) that preceded tumor regrowth at day 7 of the drug holiday (Fig. 2C). In our previous studies, E2F levels did not dramatically increase in 1205Lu tumors from mice treated with control diet over the course of 23 days (9), thus suggesting that E2F reactivation is frequently associated with therapeutic resistance (Supplementary Fig. S3).

Differential Signaling Pattern Across Scheduling Arms

To investigate the resistance mechanism to MEKi–CDK4/6i combinations, we performed reverse-phase protein array (RPPA) analysis on tumor samples (11). Unsupervised hierarchical clustering sorted the samples into three distinct groups with a high degree of clustering of resistant tumors within each scheduling group (Fig. 3A). RPPA analysis revealed that continuous MEKi plus intermittent CDK4/6i–resistant tumors (#1 and #2) and the continuous CDK4/6i plus intermittent MEKi–resistant tumor (#1) were associated with maintenance of the MEK–ERK1/2 pathway and phospho-S6 levels (Fig. 3A). We validated the RPPA results by Western
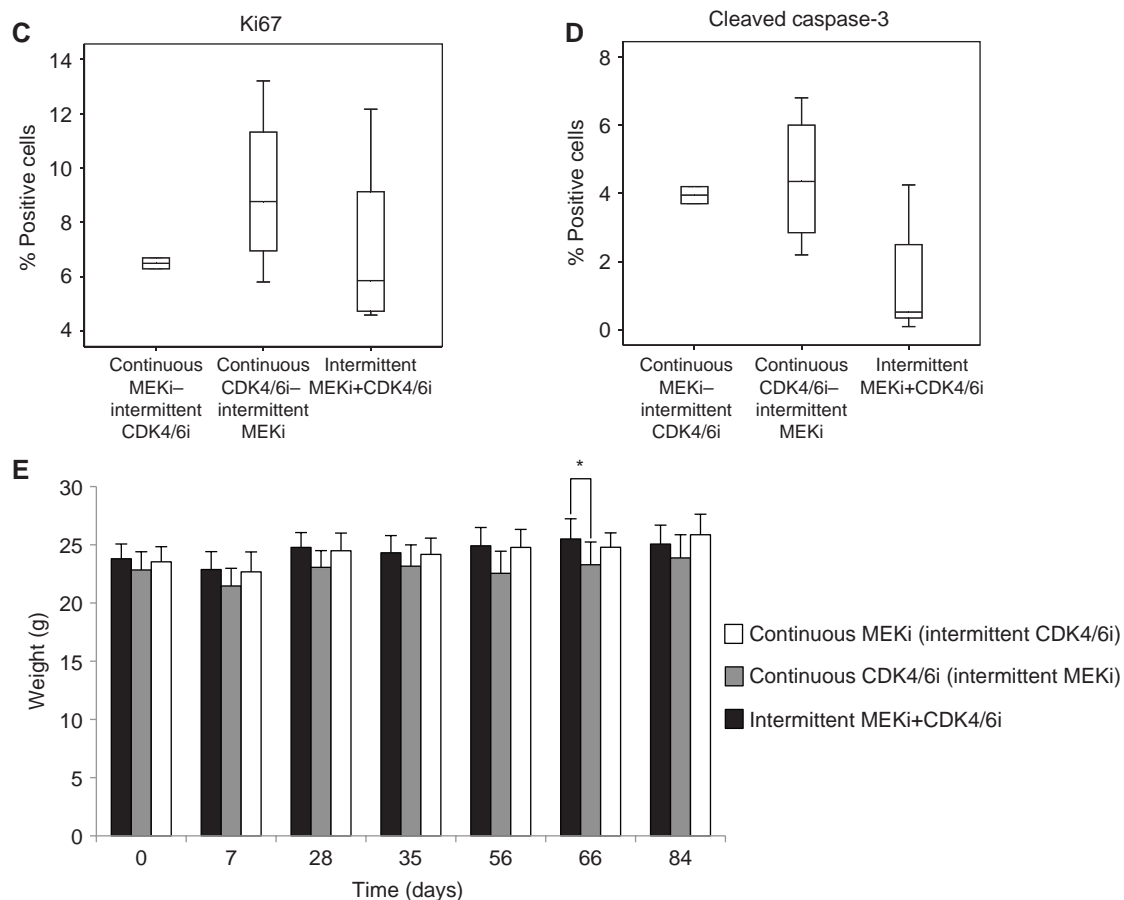
Figure 1. *(Continued)* **C,** Quantitation of Ki67-positive tumor cells taken from mice with resistant tumors (day 87) from continuous MEKi arm ($n = 2$), continuous CDK4/6i arm ($n = 3$), and intermittent MEKi + CDK4/6i arm ($n = 6$). **D,** Quantitation of cleaved caspase-3–positive tumor cells taken from mice with resistant tumors (day 87) from continuous MEKi arm ($n = 2$), continuous CDK4/6i arm ($n = 3$), and intermittent MEKi + CDK4/6i arm ($n = 6$). **E,** Average weight (g) of mice bearing 1205Lu xenografts treated in each cohort ($n = 8$, error bars, SD; *, $P < 0.05$).

American Association for Cancer Research
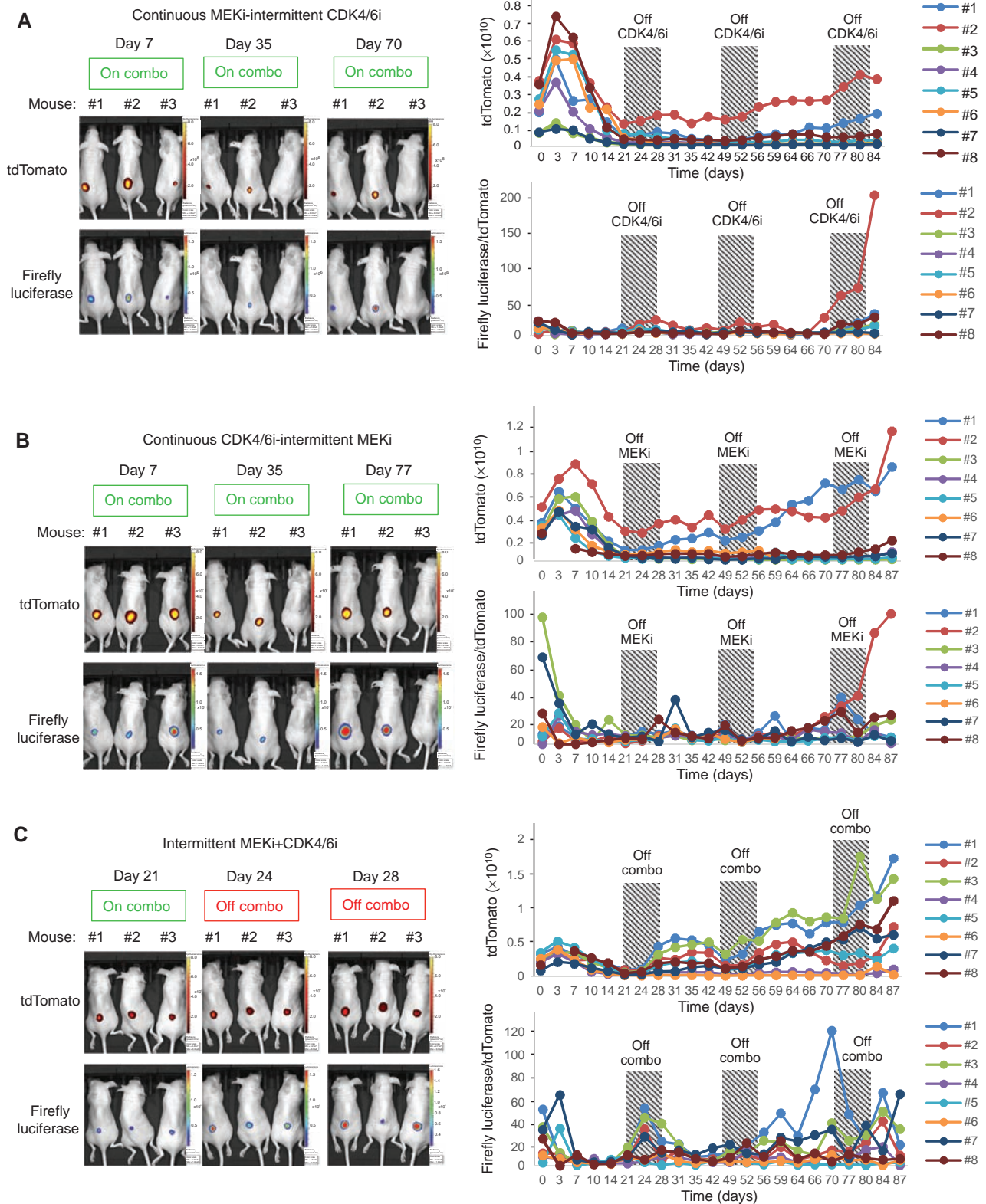
Figure 2. Utility of the E2F reporter system to determine efficacious schedules. **A,** Effect of continuous MEKi plus intermittent CDK4/6i. Longitudinal quantification of firefly luminescence representing pathway activity and tdTomato fluorescence representing tumor size. **B,** Effect of continuous CDK4/6i plus intermittent MEKi. **C,** Effect of intermittent dosing of MEKi plus CDK4/6i.
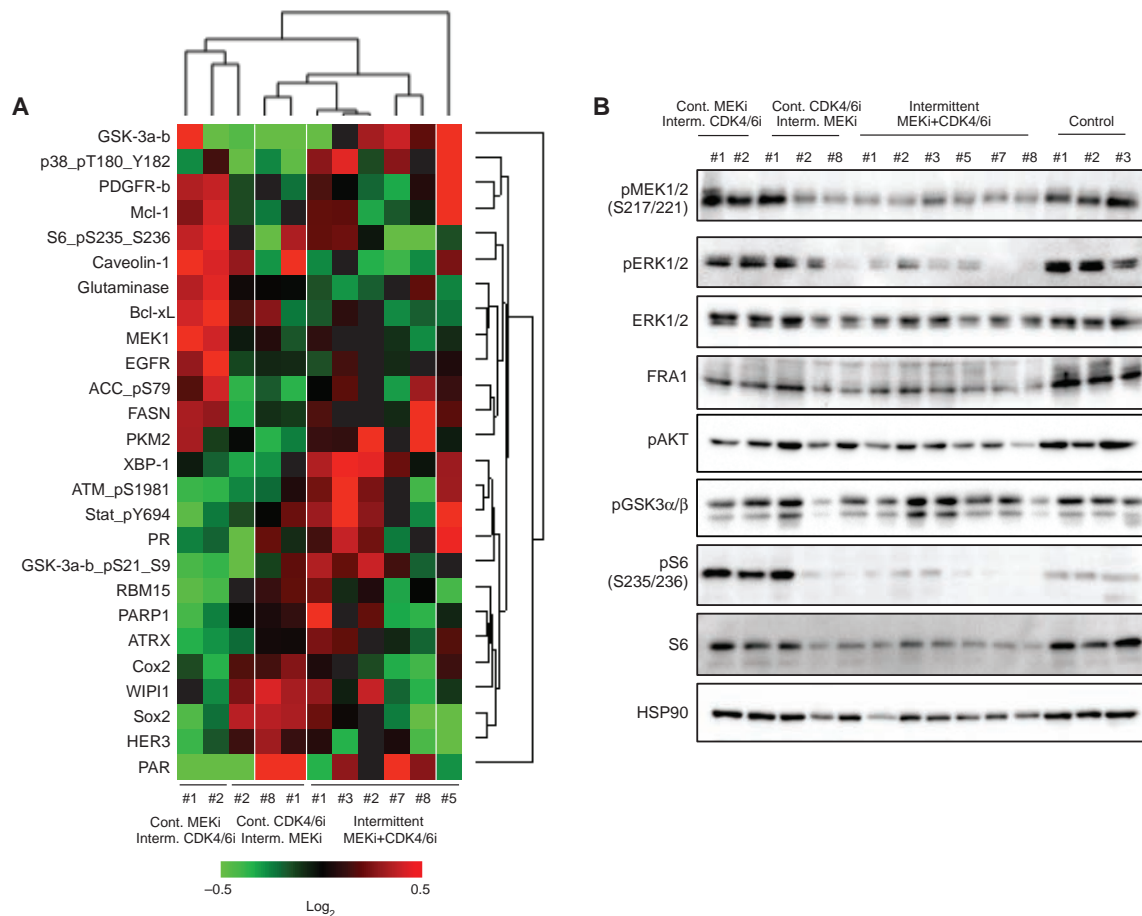
Figure 3. Pathway analysis of resistant tumors. **A,** RPPA analysis on resistant tumors. Unsupervised hierarchical clustering sorted the tumor samples into three distinct groups. Intermittent #5 clustered by itself. **B,** Western blot validation of RPPA analysis on resistant tumor lysates.

blot analysis. Notably, phospho-S6 levels were elevated above baseline of control tumors (Fig. 3B). These data implicate maintenance of MEK signaling and elevated S6 protein activity in acquired resistance to MEKi plus CDK4/6i.

Short Pulsatile CDK4/6 Inhibition Leads to Rapid Tumor Progression

To further refine drug scheduling, we compared the most effective arm with continuous MEKi plus pulsatile (4 days on, 3 days off) CDK4/6i. E2F pathway activity analysis of the pulsatile schedule showed that E2F was rapidly reactivated after each off-combination cycle (Supplementary Fig. S4A). Initially, there was no noticeable difference in tumor size between the two arms, but after 3 weeks of treatment, there was a clear separation in tumor kinetics. Tumors on continuous MEKi with pulsatile CDK4/6i progressed more rapidly, producing only one complete responder compared with the continuous MEKi with intermittent CDK4/6i schedule (Supplementary Fig. S4C). Mouse weight, hematocrit levels, and neutrophil counts were not significantly altered with the pulsatile schedule (Supplementary Figs. S2 and S4D), indicating that the schedule was well tolerated. These data indicate that prolonged dosing of CDK4/6i is more beneficial in delaying tumor growth.

Acquired Resistance to MEK and CDK4/6 Inhibition Is Associated with Enhanced S6 Phosphorylation

To extend the study of resistance to mutant NRAS melanoma, we analyzed WM1366 xenografts (ComboR1 and ComboR2) that had acquired resistance to continuous MEK and CDK4/6 inhibitor treatment (Fig. 4A). We performed RNA sequencing (RNA-seq) and targeted cancer panel sequencing on resistant tumors. Gene set variance analysis revealed distinct gene expression signatures between the two ComboR tumors, indicating heterogeneity (Supplementary Fig. S5A). Pathway analysis showed that most pathways were not uniquely regulated between ComboR1 and ComboR2; however, one of the 44 shared pathways included upregulation of an AKT pathway gene signature (Supplementary Fig. S5A and S5B). Interestingly, in ComboR1, *NRAS* was one of the most differentially upregulated genes by RNA-seq and had the highest copy-number change by targeted sequencing (Supplementary Fig. S5C; Fig. 4B). We observed high copy-number change of *NRAS* in a second WM1366-resistant tumor sample isolated from the continuous MEKi plus intermittent CDK4/6i schedule (Fig. 4B; Supplementary Fig. S5D). Furthermore, we detected high levels of *NRAS* in
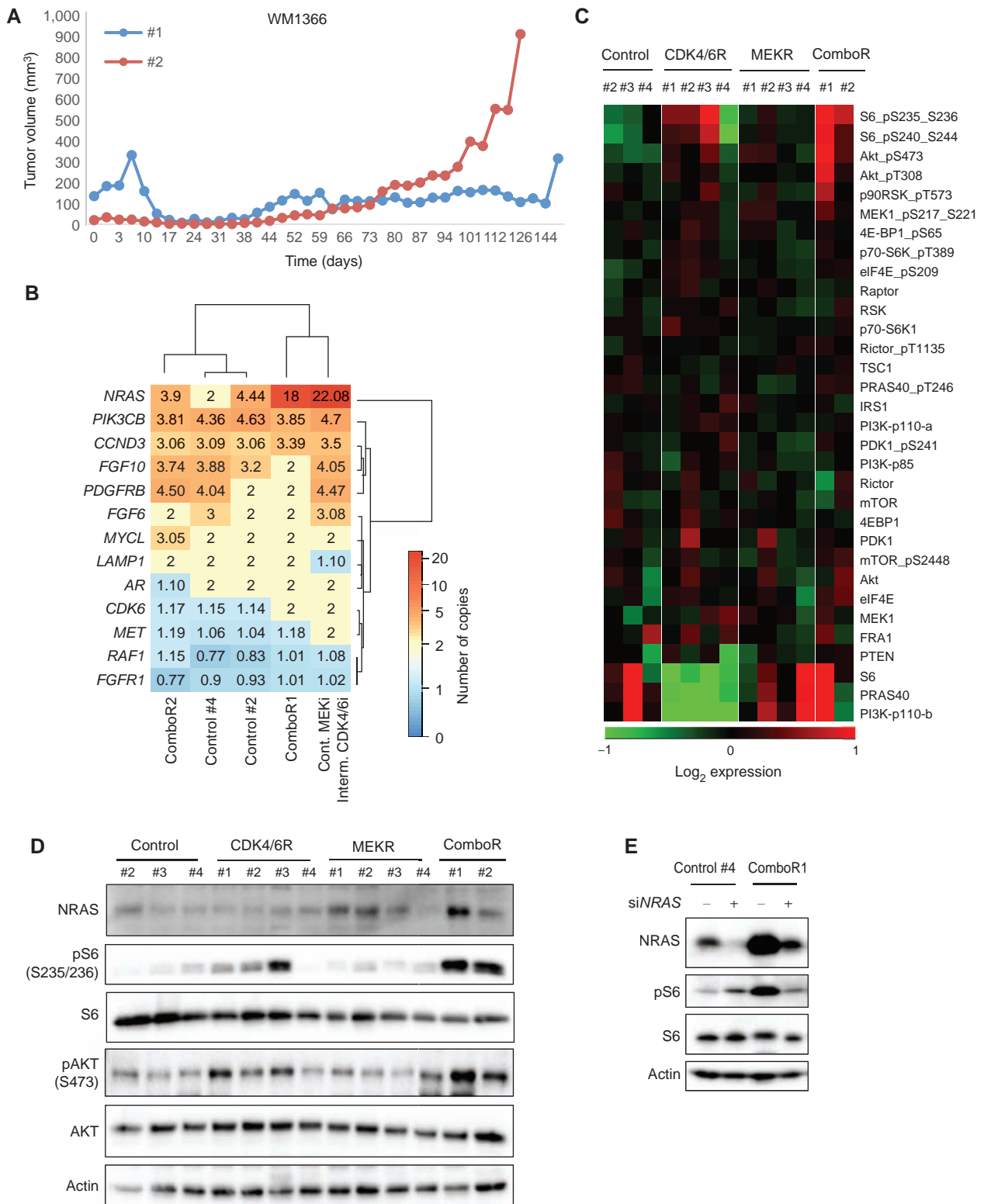
Figure 4. Mutant NRAS xenografts that acquired resistance to MEKi plus CDK4/6i show induction of mTOR activity and aberrant regulation of NRAS. **A,** WM1366 xenografts acquire resistance to continuous MEK and CDK4/6 inhibition. **B,** Identification of copy-number variations in ComboR tumors from next-generation sequencing targeting of 170 genes. **C,** Proteins and phospho-proteins involved in the activation of the mTOR pathway by RPPA analysis of resistant tumors. **D,** MEKi- and CDK4/6i-resistant tumors show induction of AKT and RPS6 activity and enhanced expression of NRAS. **E,** NRAS knockdown in ComboR1 cell line inhibits phospho-S6. Western blot analysis of cell knockdown with either control or NRAS siRNA.

ComboR1 and elevated phosphorylated AKT and S6 protein in both ComboR tumors (Supplementary Fig. S5E; Fig. 4C). We validated the enhanced levels of NRAS, phospho-AKT, and phospho-S6 in ComboR1 and ComboR2 tumors compared with tumors that progressed on vehicle by western blot analysis (Fig. 4D).

To determine whether upregulation of NRAS is required for enhanced phospho-S6, we silenced NRAS in resistant cells derived from ComboR1. Consistent with tumor samples, ComboR1 cells displayed high expression of NRAS compared with control cells (Fig. 4E). Knockdown of NRAS in ComboR1 cells dramatically reduced phospho-S6 levels, suggesting that NRAS mediates increased mTOR–S6 pathway activation (Fig. 4E). Taken together, these data indicate that distinct mechanisms are employed by melanoma tumors to circumvent MEK plus CDK4/6 inhibition, but those resistance pathways eventually converge to upregulate phosphorylation of S6 protein.

High Phospho-S6 Levels Are Associated with CDK4/6 Inhibitor Combinations in Patient Samples

To determine the clinical relevance of our findings, we analyzed levels of S6 phosphorylation in tumor samples from nine patients with mutant BRAF melanoma enrolled in two phase Ib/II clinical trials involving the triple combination of BRAFi, MEKi, and CDK4/6i (see Methods). IHC staining indicated that high phospho-S6 levels during pretreatment predicted a worse clinical outcome, but patient numbers were low and the difference did not reach statistical significance (Fig. 5A). The sets contained three patient-matched pairs of pretreatment and posttreatment samples. Importantly, there was a clear increase in phosphorylated S6 in two of the three posttreatment samples from patients who relapsed within a year on the triple therapy compared with the pretreatment sample (Fig. 5B). The patient sample (patient #3) with reduced phosphorylation of S6 posttreatment was associated with a prolonged response (421 days) to the triple combination (Fig. 5C).

To identify mechanisms of resistance associated with patients, we sequenced multiple pre- and post-CDK4/6i samples from a single patient from the LOGIC2 trial (Supplementary Fig. S6). Interestingly, we found a gain in *NRAS* mutation (Q61H and Q61L) in two of the three samples isolated from one patient post-CDK4/6i progression (Fig. 5D). To determine whether acquisition of an *NRAS* mutation in a mutant BRAF background is sufficient to modulate response to MEKi plus CDK4/6i, we utilized two mutant BRAF cell lines, WM793 and 1205Lu, exogenously expressing either Q61H or Q61L mutant NRAS (Fig. 5E). In both cell lines, constitutive expression of the mutant NRAS significantly decreased sensitivity of the cells to MEKi plus CDK4/6i (Fig. 5F). Taken together, our data suggest that upregulation of NRAS activity confers resistance to MEKi–CDK4/6i targeting. Moreover, phospho-S6 activity may be a marker of response to CDK4/6i plus targeted therapy in patients.

Enhanced Phospho-S6 Levels Are mTORC1 Dependent

To determine whether ComboR tumors show phospho-S6 dependency, we utilized cell lines from tumors (Fig. 6A;

Supplementary Fig. S7A). ComboR cells in culture exhibited a modest preference for low doses of MEKi plus CDK4/6i with slightly enhanced growth rates (Fig. 6A). In the absence of drug, ComboR cells displayed a similar proliferative capacity as control #4 cells isolated from WM1366 tumors progressing on control diet (Supplementary Fig. S7B and S7C). S6 phosphorylation can be regulated by multiple pathways (12). Treatment with either the allosteric mTORC1 inhibitor rapamycin, the dual mTORC1/2 kinase inhibitor AZD2014, or the β-sparing PI3K inhibitor GDC-0032 effectively reduced S6 phosphorylation in ComboR cells (Fig. 6B). BY719, a PI3Kα inhibitor, modestly reduced S6 phosphorylation. Furthermore, knockdown of the mTORC1 component Raptor diminished S6 phosphorylation, whereas depletion of the mTORC2 component Rictor had only modest effects (Fig. 6C). Treatment with either a PI3Kβ-selective inhibitor (TGX221), a PI3Kδ/γ inhibitor (IPI-145), an ERK1/2 inhibitor (SCH-772984), or a RSK inhibitor (SL0101) did not reduce S6 phosphorylation (Fig. 6B). Together, these data suggest that enhanced S6 phosphorylation is mediated by the mTORC1 complex.

Inhibition of mTOR Blocks the Growth of MEKi-CDK4/6i–Resistant Tumors

Given the consistent effects with mTOR inhibitors, we focused on this class of inhibitors and utilized AZD2014 in subsequent studies, as this drug induced a more complete inhibition of the mTOR pathway than rapamycin (Fig. 6B). Notably, both ComboR1 and ComboR2 cells were more sensitive to AZD2014 monotherapy compared with parental and control cells in *in vitro* viability assays, suggesting a therapeutic window (Fig. 7A). Next, we compared the effects of single agents, double combination (MEKi and CDK4/6i), or triple combination (MEKi, CDK4/6i, and AZD2014) in ComboR cells. Western blot analysis showed that AZD2014 inhibited phospho-S6 levels in both parental and ComboR cells but that the triple combination was required for efficient RB dephosphorylation in ComboR cells (Supplementary Fig. S8A). By colony formation assay, we confirmed that ComboR cells were more sensitive to AZD2014 alone than parental cells (Fig. 7B). Furthermore, the triple combination completely ablated colony formation in ComboR cells (Fig. 7B). Similar inhibitory effects were seen by inclusion of either MEKi or CDK4/6i alone plus AZD2014 by MTT assay (Fig. 7C; Supplementary Fig. S8B). Increased apoptosis was observed with the triple drug treatment compared with MEKi plus CDK4/6i or AZD2014 alone treatments in ComboR cells, suggesting that combined mTORC1/2 inhibition with MEKi/CDK4/6i may be more effective in decreasing cell viability and inducing cell death (Fig. 7D). In contrast, mTORC1/2 inhibition alone did not induce cell death in control #4 cells (Fig. 7D).

Finally, we tested the effect of mTORC1/2 inhibition on MEKi–CDK4/6i-resistant xenografts. ComboR1 cells displayed short latency and aggressive growth *in vivo* compared with control #4 cells (Supplementary Fig. S9A). Given the potential for toxicity, we utilized an intermittent AZD2014 dosing schedule (twice daily, 2 days on/5 days off) previously shown to be as efficacious as chronic daily dosing in xenograft models and associated with lower toxicities (13). We confirmed that Combo-resistant tumors were sensitive
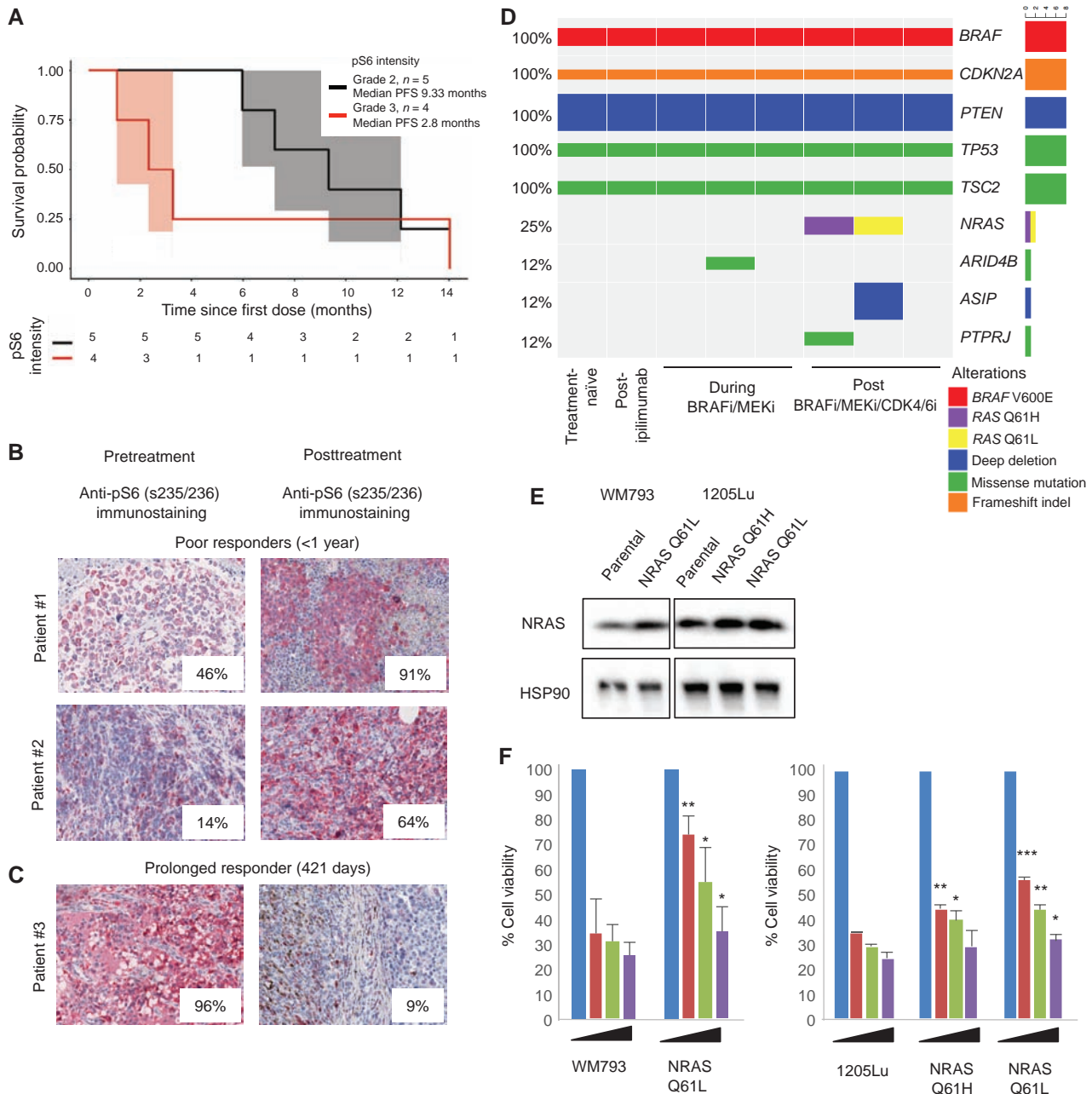
Figure 5. Increased phospho-S6 in patient samples following progression on BRAFi/MEKi/CDK4/6i. **A,** Kaplan–Meier survival curve of patients with melanoma treated with triple inhibitor combination targeting BRAF (LGX818), MEK (MEK162), and CDK4/6 (LEE011) sorted by intensity of phospho-S6 activity in pretreatment samples. Low activity, grade 2; high activity, grade 3. PFS, progression-free survival. **B** and **C,** Immunostaining of S6 phosphorylation in poor responding and prolonged responding matched pairs of melanoma samples before and relapsed under triple inhibitor combination targeting BRAF (LGX818), MEK (MEK162), and CDK4/6 (LEE011). **D,** Oncoprint depicting alterations and comutations in pretreatment and posttreatment samples from a single mutant BRAF patient in the LOGIC2 trial. **E,** Mutant BRAF cells WM793 and 1205Lu with constitutive expression of mutant NRAS (Q61H and Q61L). **F,** Mutant BRAF cells coexpressing mutant NRAS (Q61H and Q61L) are less sensitive to MEKi and CDK4/6i (error bars = SD, $n = 3$, *, $P < 0.05$; **, $P < 0.005$; ***, $P < 0.0005$).

to mTORC1/2 inhibitor alone *in vivo* (Fig. 7E). However, the tumors eventually progressed, and all mice had to be sacrificed within 2 weeks. No significant weight loss was observed with intermittent AZD2014 dosing (Supplementary Fig. S9B).

Mice bearing ComboR1 tumors treated with MEKi plus CDK4/6i showed similar tumor growth as those treated with control diet (Fig. 7F). In contrast, inclusion of intermittent

doses of AZD2014 led to a significant suppression of tumor growth (Fig. 7F) and improved mouse survival (Fig. 7G). This was also reflected in increases in apoptotic markers, cleaved caspase-3 and PARP, and decreased Ki67 staining following triple drug treatment (Fig. 7H; Supplementary Fig. S10). Taken together, these data suggest that the mTOR pathway mediates acquired resistance to the combination of MEK and
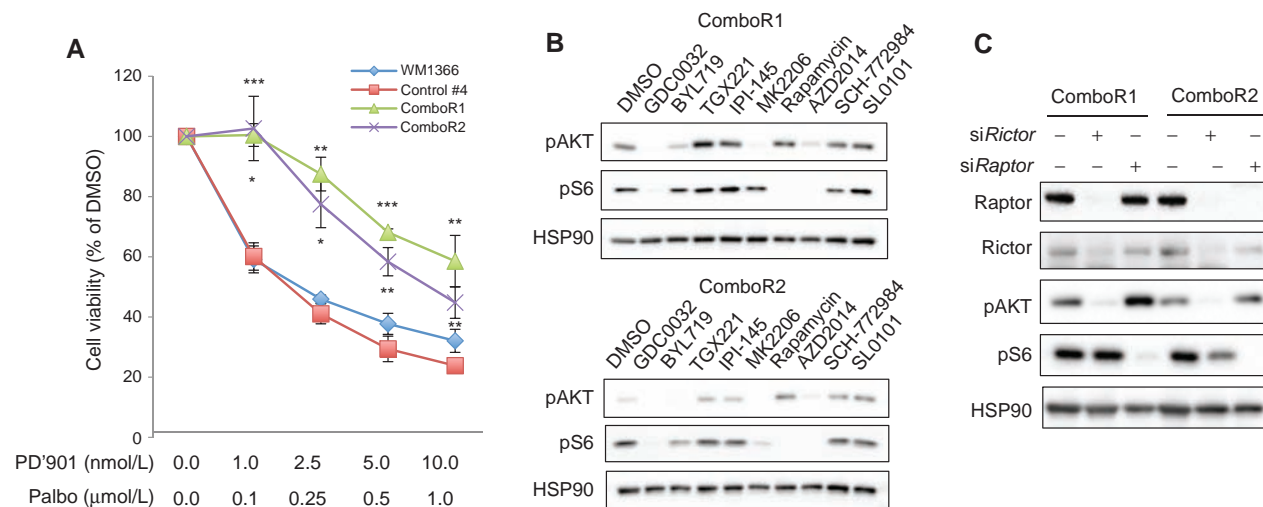
Figure 6. Inhibition of mTOR reduces S6 phosphorylation in ComboR cells. **A,** WM1366 ComboR cells are resistant to MEKi (PD'901) and CDK4/6i (palbociclib) *in vitro* by MTT assay (error bars = SD, $n = 3$, *, $P < 0.05$; **, $P < 0.005$; ***, $P < 0.0005$). Cells were treated for 7 days. **B,** Effects of PI3K/AKT/mTORC1-2/ERK inhibitors (1 µmol/L) on RPS6 activity in ComboR cells. **C,** Effects of knockdown of mTORC1 and mTORC2 components Raptor and Rictor on phospho-S6 activity.

CDK4/6 inhibition through the enhanced phosphorylation of S6, which can be blocked with an mTORC1/2 inhibitor.

DISCUSSION

The recent clinical approval of multiple CDK4/6 inhibitors and frequent alterations in components of the CDK4/6 pathway in melanoma support the rapid interrogation and optimization of these agents in this disease and raise questions regarding how they may be leveraged in combination with other targeted therapies. Using a quantitative *in vivo* reporter model to test scheduling of combinations, we show that continuous MEKi dosing with intermittent CDK4/6i yields more effective tumor inhibition than alternative intermittent scheduling options. Nevertheless, some tumors ultimately acquire drug resistance. Our studies demonstrate that this resistance is associated with aberrant regulation of NRAS and enhanced phosphorylation of S6 in both xenografts and patient samples (Supplementary Fig. S11). Taken together, these data suggest that mTORC1/2 inhibitors may serve as a salvage option for MEKi–CDK4/6i-resistant disease.

CDK4/6i lead to cytostatic effects and the addition of MEKi enhances tumor apoptosis in melanoma (9). However, alternative dosing schedules are required to potentially alleviate toxicities observed in early-phase clinical trials with continuous dosing of MEKi and CDK4/6i. Furthermore, reversible drug-tolerant states or adaptive mechanisms exist before the acquisition of permanent resistance and can be exploited (14–16). Similarly, discontinuous dosing or drug holidays may also present a disadvantage for cells that are addicted to drug (17). In our ComboR models, we observed a modest drug preference rather than an addiction phenotype in resistant cells, as these cells continue to proliferate *in vitro* and grow aggressively *in vivo* even in the absence of drug. Recent mechanistic studies involving BRAFi addiction

show that drug holidays could benefit from a second targeted inhibitor that could augment the addiction phenotype (18). Tumor progression in the intermittent scheduling arm (1-week drug holiday) was associated with rapid E2F reactivation and tumors were tolerant to subsequent retreatment. The best arm (continuous MEKi-intermittent CDK4/6i) would alleviate a major toxicity, as neutropenia induced by palbociclib is often reversible and resolved with a 1-week-off cycle (19). Our scheduling study is relevant for other tumor types, as combinations involving MEKi and CDK4/6i show promise in PDX models of mutant KRAS–driven colorectal cancer (20) and mutant KRAS non–small cell lung cancer xenografts (21).

We propose that acquired resistance to MEKi–CDK4/6i combination is associated with enhanced phosphorylation of S6. These results complement studies in other tumor models. PDK1, a kinase required for full activation of AKT and other AGC kinases, is upregulated with short-term palbociclib treatment in breast cancer models (22). Also, the induction of metabolic activity via mTOR pathway may serve as a CDK4/6i resistance mechanism in pancreatic cancer (23). Although we did not detect alterations in Raptor associated with resistance, this mTORC1 component has been implicated in palbociclib-induced senescence (24) and our data do not implicate mTORC2 in resistance (Fig. 6C; ref. 25). Of note, *PI3KCA*, which is frequently mutated and can sustain cell proliferation via the mTORC1–S6 node (26), was wild-type in our posttreatment patient samples (Supplementary Fig. S12).

Mechanistically, sequencing of mutant NRAS MEKi–CDK4/6i-resistant xenograft samples revealed heterogeneous genetic and transcriptomic features. For example, NRAS was overexpressed in two of three resistant xenografts sequenced. However, all three tumor samples had high phospho-S6 levels, suggesting a common downstream node for resistance and that mTOR pathway activation can be also driven
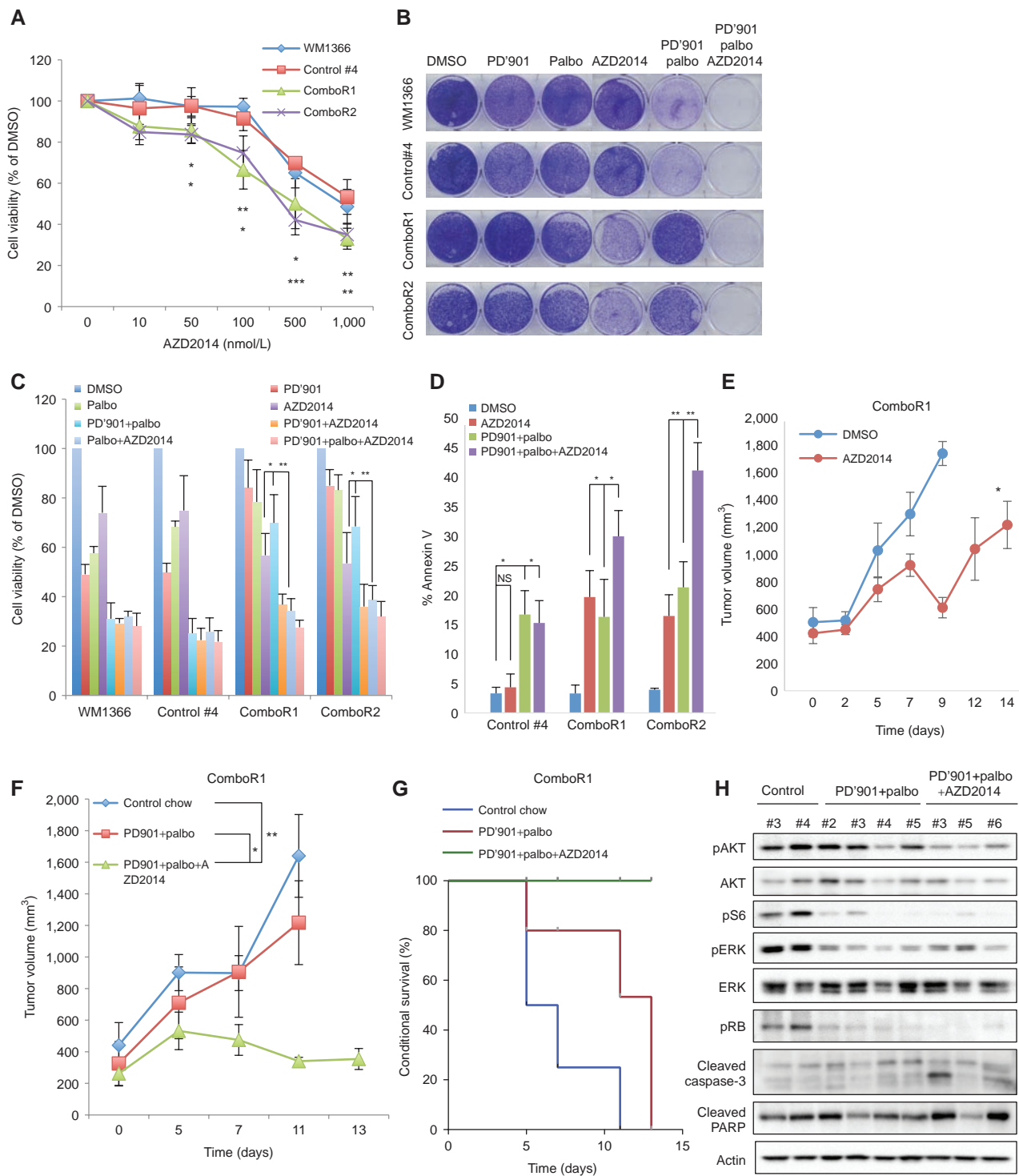
Figure 7. mTORC1/2 inhibitor enhances the effects of MEKi plus CDK4/6i in resistant cells. **A,** WM1366 ComboR cells show increased sensitivity to mTORC1/2 inhibitor AZD2014 compared with parental and control cells (error bars = SD, $n = 3$, *, $P < 0.05$; **, $P < 0.005$; ***, $P < 0.0005$). Cells were treated for 7 days and analyzed by MTT assay. **B,** The triple targeting of MEK, CDK4/6, and mTORC1/2 has greater efficacy in ComboR cells by colony formation assay. **C,** As per **B,** but MTT assays were performed (error bars = SD, $n = 3$, *, $P < 0.05$; **, $P < 0.005$). **D,** The triple targeting of MEK, CDK4/6 and mTOR led to increased apoptosis in ComboR cells by Annexin V staining (*, $P < 0.05$; **, $P < 0.005$). **E,** WM1366 ComboR1 xenografts were treated with vehicle or AZD2014 (20 mg/kg, 2/5 days; error bars = SEM, $n = 4$; vehicle, $n = 5$; AZD2014, *, $P = 0.009$). **F,** WM1366 ComboR1 xenografts were treated with control chow, combination chow (PD'901 and palbociclib), and combination chow plus AZD2014 (20 mg/kg, 2/5 days by oral gavage; error bars = SEM, $n = 4$; control, $n = 4$; combo, $n = 3$; combo+AZD2014, *, $P < 0.05$; **, $P < 0.005$). **G,** Kaplan–Meier curve of data in **F** shows significant survival advantage of AZD2014 inclusion in ComboR1 xenografts ($P < 0.05$). The endpoint for euthanasia was predetermined as 1,000 mm³ tumor volume. **H,** Analysis of downstream targets regulated by the combination chow (PD'901 and palbociclib) and combination chow plus AZD2014.

by mechanisms other than NRAS. In CDK4/6i-progressing mutant BRAF patient samples, we detected *NRAS* mutations in two of three samples, pointing at heterogeneous mechanisms within a single patient. It is possible that intratumoral heterogeneity exists within patient samples that may be circumvented with multiregion sampling (26). Our findings are in line with upregulation of oncogene activity as a mode of resistance to targeted therapies (27).

Although multiple mechanisms may exist in upregulating the mTOR pathway during the acquisition of resistance, importantly, the convergence upon the S6 node allows for the utility of AZD2014 or similar mTORC inhibitors that may serve as a salvage option. Unlike rapalogs, AZD2014 inhibits kinase activity of both mTORC1 and mTORC2, to induce a more complete inhibition of the pathway (13), and is currently in phase II trials for advanced solid tumors and clear cell renal cancer (28). The elevated S6 phosphorylation associated with resistance and the effect of 2-day AZD2014 treatment in preclinical models of resistance warrant further longitudinal studies to analyze the effects of the mTORC1/2 inhibitor sequencing schedules interlaced with MEKi–CDK4/6i therapies.

METHODS

Cell Culture

1205Lu and WM1366 cells were transduced with E2F-EGFP-firefly luciferase as described previously (9). 1205Lu and WM1366-reporter cells were cultured in MCDB153 (Sigma) with 2% FBS, 20% Leibowitz L-15 medium, and 5 μg/mL insulin. WM1366 and 1205Lu cells were donated by Dr. Meenhard Herlyn (Wistar Institute, Philadelphia, PA) in 2005. Cell lines were authenticated by sequencing at the NRAS, BRAF, and CDK4 loci, and by STR analysis (completed April 2015).

Reagents

Palbociclib (PD0332991) was generously provided by Pfizer, Inc. PD0325901, AZD2014, rapamycin, GDC0032, BYL719, TGX221, IPI145, and SCH772984 were purchased from Selleck Chemicals. SL0101 was purchased from Millipore. Collagenase was purchased from Sigma.

Western Blot Analysis

Protein lysates were prepared in Laemmli sample buffer, separated by SDS page, and proteins transferred to a PVDF membrane. Immunoreactivity was detected using horseradish protein conjugate secondary antibodies (CalBioTech) and chemiluminescence substrate (Thermo Fisher Scientific) on the Versadoc Imaging System (Bio-Rad). The following primary antibodies were utilized: phospho-RB1 (S780; #9307), RB1 (#9309), phospho-ERK1/2 (#9101), ERK1/2 (#9102), phospho-S6 Ribosomal Protein (S235/236; #4857), S6 (#2217), phospho-MEK1/2 (Ser217/221; #9121), pAKT (S473; #4060), AKT (#9272), HSP90 (#4877), Rictor (#2114), Raptor (#2280), cleaved caspase-3 (#9661), and cleaved PARP (#9541), all purchased from Cell Signaling Technology; NRAS (sc31 and sc519) and Fra-1 (sc605) were purchased from Santa Cruz Biotechnology, Inc.; actin (A2066) was purchased from Sigma-Aldrich Co.

RPPA Analysis

Tumors were lysed in RPPA lysis buffer and analyzed as described previously (9). Tumors analyzed in Figs. 3 and 4C were all isolated at the same time point at day 87 and the final time point shown in the tumor kinetics graph, respectively. All mice were kept on drug during the day of isolation. Comparisons of normalized RPPA data were performed between groups by the two-sample t test method

with 1,000 permutations and assumed unequal variance. A $P <$ 0.05 and fold change >50% were used as cutoffs for determining significance. Unsupervised and supervised hierarchical clustering heat maps were produced using $\log_2$-transformed sample expression data for antibody lists constructed from either significance cutoffs or *a priori* pathway information. Calculations were performed using Matlab (v2017b).

Targeted Sequencing

Targeted sequencing was performed using the Illumina TruSight Tumor 170 Targeted Panel that covers all annotated coding exons for 170 genes implicated in cancer etiology and pathways. Sequencing libraries were prepared per the manufacturer's recommendation. Sequencing was performed on the Illumina NextSeq 500 platform with 2×100 base paired-end reads at an average depth of approximately 90 M reads per sample. Base calls were converted to FASTQ format on the Illumina cloud-based BaseSpace platform. The BaseSpace TruSight Tumor 170 App Version 1.0.1 was then used to align reads to the human reference genome version hg19 with the Isaac Aligner, perform local realignment around indel calls, call small variants using the Illumina Pisces algorithm, and detect deletions/amplifications using the Illumina CRAFT (CNV Robust Analysis For Tumors) copy number variant caller. Variant call annotation was performed using ANNOVAR software version 2017jun01 (29). An unsupervised hierarchical clustering heat map was generated from CRAFT amplification and deletion copy-number variation call data for alterations found in at least one drug-resistant sample. The targeted sequencing results have been deposited in the NCBI Sequence Read Archive (SRA) database under accession number SRP133305.

siRNA Transfection

Cells were transfected as described previously (9). *NRAS*-specific siRNA (#D-003919-02) sequence is as follows: CAAGUGUGAUU UGCCAACA. Raptor-specific siRNA (#D-004107-01-0005) sequence is as follows: GAAACCAUCGGUGCAAAUU. Rictor-specific siRNA (#D-016984-01-0005) specific sequence is as follows: UCAACGAG CUCACAUAUGA.

Melanoma Patient Samples

Patient studies were conducted according to the Declaration of Helsinki, and informed consent was obtained from all patients. Tumor samples were collected and analyzed according to University of Zurich Institutional Review Board–approved protocols (EK647 and EK800). Patient samples were collected from the following trials. For NCT01543698, BRAFi and MEKi (LGX818 and MEK162) were administered on a continuous schedule and CDK4/6i (LEE011) was administered in a 3-week-on, 1-week-off schedule. For NCT02159066 (LOGIC2), patients progressing on BRAFi and MEKi (LGX818 and MEK162) were treated with CDK4/6i (LEE011).

Sequencing of Patient Samples

One patient from the LOGIC2 trial (NCT02159066) had tumor biopsies collected before combination therapy, during encorafenib and binimetinib therapy, and after encorafenib, binimetinib, and ribociclib triple combination therapy (informed consent obtained; protocol number: EK647 and EK800). Melanoma cell cultures were established from the biopsies and submitted for targeted panel sequencing. Samples were subjected to 150 bp paired-end sequencing on an Illumina HiSeq4000. Raw reads were trimmed for adaptors and quality by trimmomatic (30) and aligned with bwa mem (31). Aligned reads were processed by the GATK best practices for somatic mutation calling (version 3.7; ref. 32), and variants were annotated with the Variant Effect Predictor (33).

IHC Analysis of Patient Samples for Phospho-S6

Sections were stained with anti–phospho-S6 (Ser235/236; antibody #4858 from Cell Signaling Technology). For quantitation of the slides, five to six representative areas per slide were analyzed using Aperio eSlide Manager software in a blinded manner by a board-certified pathologist (K. HooKim). To generate the patient survival curve, grading scores of pretreatment samples were based on the following readout: grade 3 >80% positive, grade 2 >40%–80% positive, grade 1 = 1%–40%.

IHC Analysis for Ki67 and Cleaved Caspase-3

Tissue were fixed in formalin and paraffin embedded. Sections were stained with anti-Ki67 (1:150) and cleaved caspase-3 (1:300) antibody. The intensity of staining and the percentage of positive cells were evaluated in a blinded manner using the Aperio ScanScope XT slide scanning system, and quantification was done with the Aperio eSlide Manager software. Five representative areas (×200 magnification) per slide were analyzed. Ki67 antibody (MA1-90584) was purchased from Thermo Fisher Scientific, and cleaved caspase-3 antibody (#9661) was purchased from Cell Signaling Technology.

In Vivo Experiments

All studies were reviewed and approved by the Institutional Animal Care and Use Committee at Thomas Jefferson University (Philadelphia, PA). For scheduling studies, mice bearing 1205Lu reporter xenografts (50–100 mm³) were fed with combination chow (AIN-76A diet with 7 mg/kg PD0325901 and 429 mg/kg palbociclib, $n = 8$.cohort) for 3 weeks and then switched to single agent (AIN-76A with 429 mg/kg palbociclib or AIN-76A with 7 mg/kg PD0325901) or control diet (AIN-76A) for one week. For therapeutic window studies, mice bearing WM1366 control #4 or ComboR1 xenografts were fed with control diet or control diet plus AZD2014 administered by oral gavage bi-daily (2 days on, 5 days off). AZD2014 was dissolved in DMSO to a final concentration of 20 mg/kg. Control and combination chow arms received DMSO alone by oral gavage. For triple combination study, mice with WM1366 ComboR1 xenografts were fed with either control diet, combination chow, or combination chow plus AZD2014. AZD2014 was administered by oral gavage bi-daily (2 days on, 5 days off) for the first week then once daily, twice a week for the second week. Digital caliper and firefly luciferase measurements were carried out as described previously (9).

Generation of Resistant Lines

Combination PD0325901- and palbociclib-resistant lines were generated from WM1366 xenograft tumors. Resistant tumors were isolated, and cells were dissociated using collagenase and continuously cultured in the presence of low-dose PD0325901 and palbociclib.

Annexin V Staining

After indicated treatments, cells were resuspended in binding buffer and stained with Annexin V-APC for 15 minutes. Apoptotic cells were analyzed by flow cytometry on the LSRII (BD Biosciences). Data were analyzed using FlowJo software (TreeStar Inc.).

MTT Assay

Analysis was carried out as described previously (9). At indicated time points, thiazolyl blue tetrazolium bromide (Sigma) was added to growth medium, incubated for 4 hours, and then solubilized overnight with 10% SDS/0.1 N HCl.

Statistical Analysis

In vitro data were analyzed using a two-tailed *t* test assuming unequal variance, with error bars representing SD. *In vivo* statistical analysis is described in Supplementary Materials and Methods.

Disclosure of Potential Conflicts of Interest

J.L.F. Teh has ownership interest in U.S. Patent 9880150. M.A. Davies reports receiving commercial research grants from AstraZeneca, GSK, Merck, Oncothyreon, Roche/Genentech, and Sanofi Aventis, and is a consultant/advisory board member for GSK, Novartis, Roche/Genentech, Sanofi Aventis, Syndax, and Vaccinex. L.N. Kwong reports receiving a commercial research grant from Array Biopharma. M.P. Levesque reports receiving commercial research grants from Bristol Meyers Squibb, Novartis, and Roche. R. Dummer received research funding from Novartis, Merck Sharp & Dhome (MSD), Bristol-Myers Squibb (BMS), Roche, and GSK, and has a consultant or advisory board relationship with Novartis, MSD, BMS, Roche, GSK, and Amgen. A.E. Aplin reports receiving a commercial research grant from Pfizer and has ownership interest in patent number 9880150. No potential conflicts of interest were disclosed by the other authors.

Authors' Contributions

Conception and design: J.L.F. Teh, L.N. Kwong, A.E. Aplin
Development of methodology: J.L.F. Teh, N. Nikbakht, P.M. Fortina, A.E. Aplin
Acquisition of data (provided animals, acquired and managed patients, provided facilities, etc.): J.L.F. Teh, P.F. Cheng, N. Nikbakht, P. Patel, P.M. Fortina, I. Kleiber, K. HooKim, M.A. Davies, M.P. Levesque, R. Dummer
Analysis and interpretation of data (e.g., statistical analysis, biostatistics, computational analysis): J.L.F. Teh, P.F. Cheng, T.J. Purwin, N. Nikbakht, I. Chervoneva, A. Ertel, R. Dummer, A.E. Aplin
Writing, review, and/or revision of the manuscript: J.L.F. Teh, P.F. Cheng, P.M. Fortina, M.A. Davies, L.N. Kwong, R. Dummer, A.E. Aplin
Administrative, technical, or material support (i.e., reporting or organizing data, constructing databases): P. Patel, A.E. Aplin
Study supervision: J.L.F. Teh, P.M. Fortina, A.E. Aplin

REFERENCES

1. Sherr CJ, Beach D, Shapiro GI. Targeting CDK4 and CDK6: from discovery to therapy. Cancer Discov 2016;6:353–67.
2. Sheppard KE, McArthur GA. The cell-cycle regulator CDK4: an emerging therapeutic target in melanoma. Clin Cancer Res 2013;19:5320–8.
3. Shapiro GI, Hilton J, Gandi L, Chau N, Cleary J, Wolanski A, et al. Phase I dose escalation study of the CDK4/6 inhibitor palbociclib in combination with the MEK inhibitor PD-0325901 in patients with RAS mutant solid tumors. In: Proceedings of the American

Association for Cancer Research Annual Meeting 2017; 2017 Apr 1–5; Washington, DC. Philadelphia (PA): AACR. Abstract nr CT046.

4. Sosman JA, Kittaneh M, P. J. K Lolkema M, Postow MA, Schwartz G, Franklin C, et al. A phase 1b/2 study of LEE011 in combination with binimetinib (MEK162) in patients with NRAS-mutant melanoma: early encouraging clinical activity. J Clin Oncol 2014;32:5s.

5. Sullivan RJ, Amaria RN, Lawrence DP, Brennan J, Leister C, Singh R, et al. Phase 1b dose-escalation study of trametinib (MEKi) plus palbociclib (CDK4/6i) in patients with advanced solid tumors. In: Proceedings of the AACR-NCI-EORTC International Conference: Molecular Targets and Cancer Therapeutics; 2015 Nov 5–9; Boston, MA. Philadelphia (PA): AACR. Abstract nr PR06.

6. Schwartz GK, LoRusso PM, Dickson MA, Randolph SS, Shaik MN, Wilner KD, et al. Phase I study of PD 0332991, a cyclin-dependent kinase inhibitor, administered in 3-week cycles (Schedule 2/1). Br J Cancer 2011;104:1862–8.

7. Basile KJ, Abel EV, Dadpey N, Hartsough EJ, Fortina P, Aplin AE. In vivo MAPK reporting reveals the heterogeneity in tumoral selection of resistance to RAF inhibitors. Cancer Res 2013;73:7101–10.

8. Hirata E, Girotti MR, Viros A, Hooper S, Spencer-Dene B, Matsuda M, et al. Intravital imaging reveals how BRAF inhibition generates drug-tolerant microenvironments with high integrin beta1/FAK signaling. Cancer Cell 2015;27:574–88.

9. Teh JL, Purwin TJ, Greenawalt EJ, Chervoneva I, Goldberg A, Davies MA, et al. An in vivo reporter to quantitatively and temporally analyze the effects of CDK4/6 inhibitor-based therapies in melanoma. Cancer Res 2016;76:5455–66.

10. Finn RS, Martin M, Rugo HS, Jones S, Im SA, Gelmon K, et al. Palbociclib and letrozole in advanced breast cancer. N Engl J Med 2016;375:1925–36.

11. Li J, Zhao W, Akbani R, Liu W, Ju Z, Ling S, et al. Characterization of human cancer cell lines by reverse-phase protein arrays. Cancer Cell 2017;31:225–39.

12. Saxton RA, Sabatini DM. mTOR signaling in growth, metabolism, and disease. Cell 2017;169:361–71.

13. Guichard SM, Curwen J, Bihani T, D'Cruz CM, Yates JW, Grondine M, et al. AZD2014, an inhibitor of mTORC1 and mTORC2, is highly effective in ER+ breast cancer when administered using intermittent or continuous schedules. Mol Cancer Ther 2015;14:2508–18.

14. Smith MP, Brunton H, Rowling EJ, Ferguson J, Arozarena I, Miskolczi Z, et al. Inhibiting drivers of non-mutational drug tolerance is a salvage strategy for targeted melanoma therapy. Cancer Cell 2016;29:270–84.

15. Sharma SV, Lee DY, Li B, Quinlan MP, Takahashi F, Maheswaran S, et al. A chromatin-mediated reversible drug-tolerant state in cancer cell subpopulations. Cell 2010;141:69–80.

16. Abel EV, Basile KJ, Kugel CH III, Witkiewicz AK, Le K, Amaravadi RK, et al. Melanoma adapts to RAF/MEK inhibitors through FOXD3-mediated upregulation of ERBB3. J Clin Invest 2013;123:2155–68.

17. Das Thakur M, Salangsang F, Landman AS, Sellers WR, Pryer NK, Levesque MP, et al. Modelling vemurafenib resistance in melanoma

18. Hong A, Moriceau G, Sun L, Lomeli S, Piva M, Damoiseaux R, et al. Exploiting drug addiction mechanisms to select against MAPKi-resistant melanoma. Cancer Discov 2018;8:74–93.

19. Hu W, Sung T, Jessen BA, Thibault S, Finkelstein MB, Khan NK, et al. Mechanistic investigation of bone marrow suppression associated with palbociclib and its differentiation from cytotoxic chemotherapies. Clin Cancer Res 2016;22:2000–8.

20. Ziemke EK, Dosch JS, Maust JD, Shettigar A, Sen A, Welling TH, et al. Sensitivity of KRAS-mutant colorectal cancers to combination therapy that cotargets MEK and CDK4/6. Clin Cancer Res 2016;22:405–14.

21. Tao Z, Le Blanc JM, Wang C, Zhan T, Zhuang H, Wang P, et al. Coadministration of trametinib and palbociclib radiosensitizes KRAS-mutant non–small cell lung cancers in vitro and in vivo. Clin Cancer Res 2016;22:122–33.

22. Jansen VM, Bhola NE, Bauer JA, Formisano L, Lee KM, Hutchinson KE, et al. Kinome-wide RNA interference screen reveals a role for PDK1 in acquired resistance to CDK4/6 inhibition in ER-positive breast cancer. Cancer Res 2017;77:2488–99.

23. Franco J, Balaji U, Freinkman E, Witkiewicz AK, Knudsen ES. Metabolic reprogramming of pancreatic cancer mediated by CDK4/6 inhibition elicits unique vulnerabilities. Cell Rep 2016;14:979–90.

24. Yoshida A, Lee EK, Diehl JA. Induction of therapeutic senescence in vemurafenib-resistant melanoma by extended inhibition of CDK4/6. Cancer Res 2016;76:2990–3002.

25. Zhang J, Xu K, Liu P, Geng Y, Wang B, Gan W, et al. Inhibition of Rb phosphorylation leads to mTORC2-mediated activation of Akt. Mol Cell 2016;62:929–42.

26. Romano G, Chen P-L, Song P, McQuade JL, Liang RJ, Liu M, et al. A preexisting rare PIK3CA^{E545K} subpopulation confers clinical resistance to MEK plus CDK4/6 inhibition in NRAS melanoma and is dependent on S6K1 signaling. Cancer Discov 2018;8:556–67.

27. Shi H, Moriceau G, Kong X, Lee MK, Lee H, Koya RC, et al. Melanoma whole-exome sequencing identifies (V600E)B-RAF amplification-mediated acquired B-RAF inhibitor resistance. Nat Commun 2012;3:724.

28. Powles T, Wheater M, Din O, Geldart T, Boleti E, Stockdale A, et al. A randomised phase 2 study of AZD2014 versus everolimus in patients with VEGF-refractory metastatic clear cell renal cancer. Eur Urol 2016;69:450–6.

29. Wang K, Li M, Hakonarson H. ANNOVAR: functional annotation of genetic variants from high-throughput sequencing data. Nucleic Acids Res 2010;38:e164.

30. Bolger AM, Lohse M, Usadel B. Trimmomatic: a flexible trimmer for Illumina sequence data. Bioinformatics 2014;30:2114–20.

31. Li H, Durbin R. Fast and accurate short read alignment with Burrows-Wheeler transform. Bioinformatics 2009;25:1754–60.

32. Cibulskis K, Lawrence MS, Carter SL, Sivachenko A, Jaffe D, Sougnez C, et al. Sensitive detection of somatic point mutations in impure and heterogeneous cancer samples. Nat Biotechnol 2013;31:213–9.

33. McLaren W, Gil L, Hunt SE, Riat HS, Ritchie GR, Thormann A, et al. The ensembl variant effect predictor. Genome Biol 2016;17:122.

reveals a strategy to forestall drug resistance. Nature 2013;494:251–5.

CANCER DISCOVERY

AACR American Association for Cancer Research

In Vivo E2F Reporting Reveals Efficacious Schedules of MEK1/2−CDK4/6 Targeting and mTOR−S6 Resistance Mechanisms

Jessica L.F. Teh, Phil F. Cheng, Timothy J. Purwin, et al.

Updated version	Access the most recent version of this article at: doi:10.1158/2159-8290.CD-17-0699
Supplementary Material	Access the most recent supplemental material at: http://cancerdiscovery.aacrjournals.org/content/suppl/2018/03/01/2159-8290.CD-17-0699.DC1

E-mail alerts	Sign up to receive free email-alerts related to this article or journal.
Reprints and Subscriptions	To order reprints of this article or to subscribe to the journal, contact the AACR Publications Department at pubs@aacr.org.
Permissions	To request permission to re-use all or part of this article, use this link http://cancerdiscovery.aacrjournals.org/content/early/2018/04/11/2159-8290.CD-17-0699. Click on "Request Permissions" which will take you to the Copyright Clearance Center's (CCC) Rightslink site.